Supporting Information

Held et al. 10.1073/pnas.1419845112

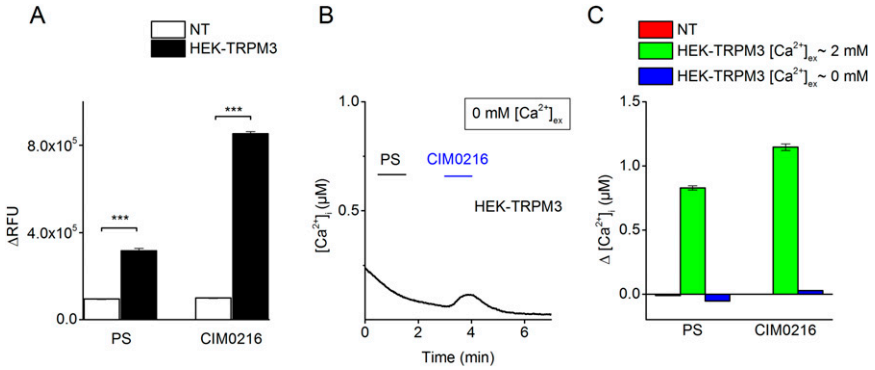

Fig. S1. Stimulation of mTRPM3 by CIM0216 induces a $[Ca^{2+}]_i$ influx derived from the extracellular medium. (*A*) Mean fluorescent increase in nontransfected HEK293 (NT) and HEK-TRPM3 cells after stimulation by PS (50 μM) and CIM0216 (10 μM). Data are mean ± SEM; $n = 4$. (*B*) Time course of Ca^{2+} imaging measurements in HEK-TRPM3 cells during application of PS (40 μM) and CIM0216 (1 μM) in the absence of extracellular calcium. $n > 500$ in at least three independent measurements. (*C*) Mean Ca^{2+} increase in HEK-TRPM3 and nontransfected (NT) HEK293 cells on stimulation with either PS (40 μM) or CIM0216 (1 μM) in the presence (2 mM) or absence of extracellular calcium.

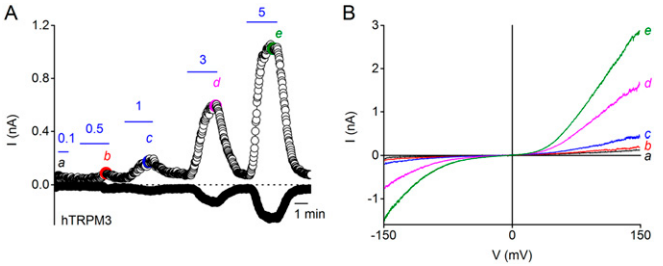

Fig. S2. CIM0216 activates human TRPM3 in a dose-dependent manner. (*A*) Time course at ±80 mV of a patch-clamp recording in whole-cell configuration showing CIM0216 dose-dependent activation of TRPM3 currents in HEK293 cells transiently transfected with human TRPM3. (*B*) I–V relationships at the time points indicated in *A*.

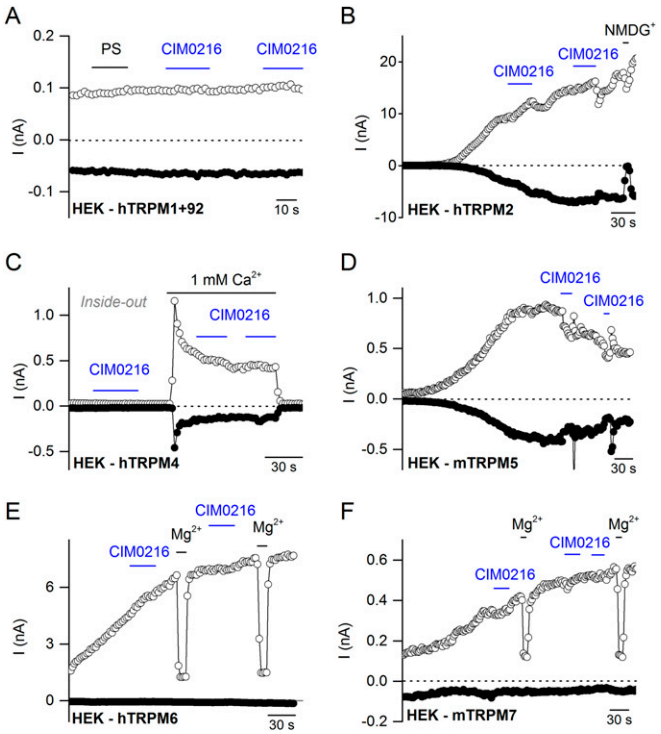

Fig. S3. Selectivity of CIM0216 against other TRPM family members. (*A*) Time course at ±80 mV of a patch-clamp recording in whole-cell configuration of HEK293 cells transiently transfected with human TRPM1. At the indicated time points, PS (40 μM) and CIM0216 (10 μM) were added. (*B*) Time course at ±80 mV of a patch-clamp recording in whole-cell configurations of HEK293 cells transiently transfected with human TRPM2. At the indicated time points, CIM0216 (10 μM) was added or all cations were exchanged for $NMDG^+$ in the extracellular solution. For activation of TRPM2, the pipette solution contained ADP-ribose (300 μM). (*C*) Time course at ±80 mV of a patch-clamp recording in an inside-out configuration of HEK293 cells stably expressing human TRPM4. At the indicated time points, CIM0216 (10 μM) was added before or during stimulation with 1 mM Ca^{2+}. (*D*) Time course at ±80 mV of a patch-clamp recording in whole-cell configuration of HEK293 cells stably expressing murine TRPM5. At the indicated time points, CIM0216 (10 μM) was added. To activate TRPM5, the pipette solution contained Ca^{2+} (1 μM), adjusted by adding appropriate amounts of $CaCl_2$ to the 10 mM EGTA-containing solution. (*E* and *F*) Time course at ±80 mV of a patch-clamp recording in whole-cell configuration of HEK293 cells transiently transfected with human TRPM6 (*E*) or murine TRPM7 (*F*). At the indicated time points, CIM0216 (10 μM) or Mg^{2+} (10 mM) was added.

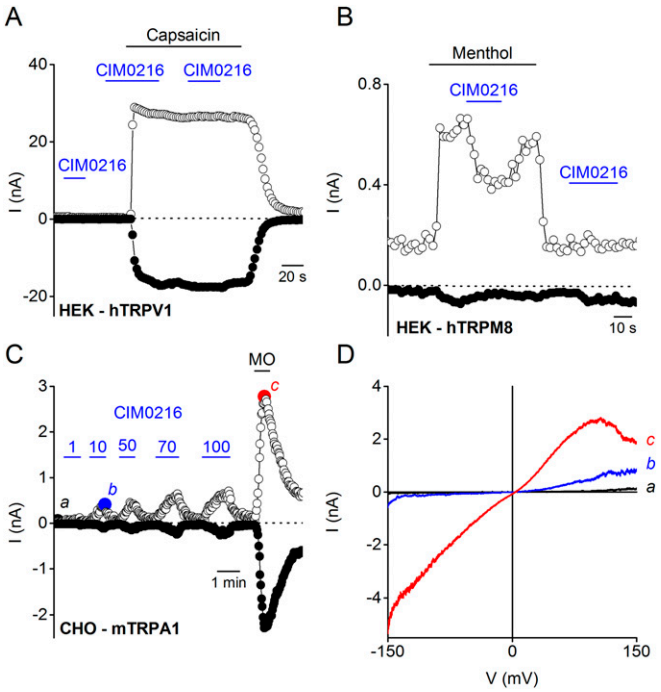

Fig. S4. Selectivity of CIM0216 against other sensory TRP channels. (*A* and *B*) Time course at ±80 mV of a patch-clamp recording in whole-cell configuration of HEK293 cells transiently transfected with human TRPV1 (*A*) and human TRPM8 (*B*). At the indicated time points, CIM0216 (10 μM) was added before or during stimulation by 1 μM capsaicin (*A*) or 100 μM menthol (*B*). (*C*) Time course at ±80 mV of a patch-clamp recording in whole-cell configuration of CHO cells stably transfected with murine TRPA1. At the indicated time points, different doses of CIM0216 (1, 10, 50, 70, and 100 μM) and MO (100 μM) were added. (*D*) I–V relationships at the time points indicated in *C*.

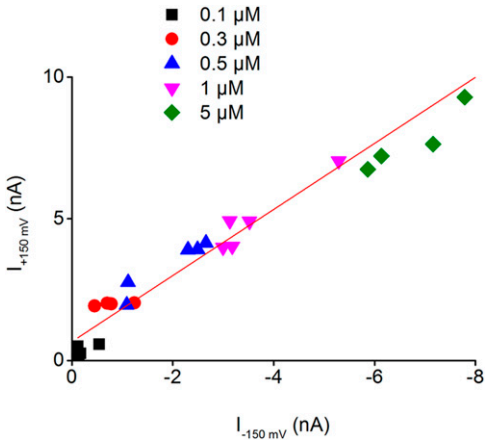

Fig. S5. The rectification pattern of CIM0216-induced TRPM3 currents is not dose-dependent. Shown are rectification patterns of CIM0216-induced TRPM3 currents at five different concentrations in HEK-TRPM3 cells, derived by plotting the currents at +150 mV against the currents at −150 mV.

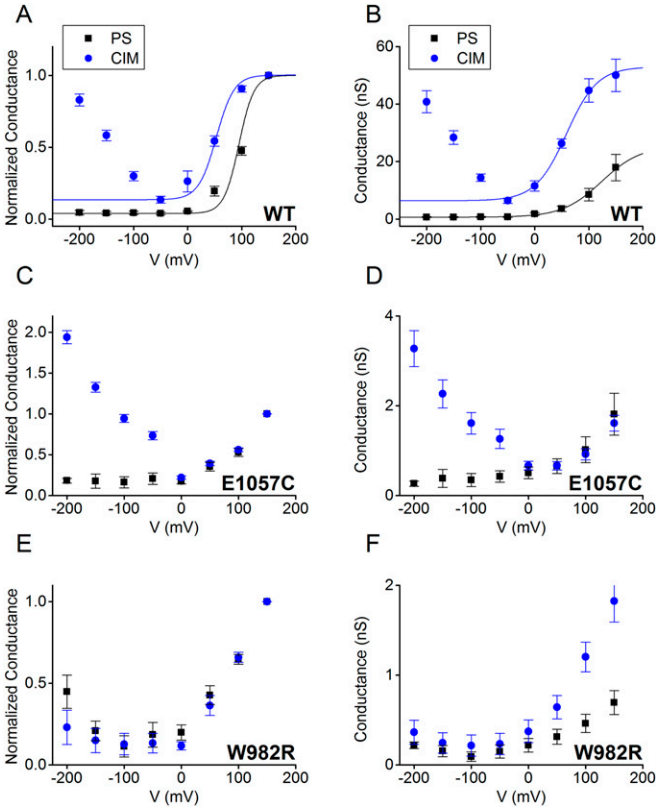

Fig. S6. Conductance curves of WT TRPM3, and TRPM3 mutant channels, in response to PS and CIM0216. (*A* and *B*) Steady-state G–V relationships obtained in HEK-TRPM3 cells in the presence of CIM0216 (1 μM) or PS (40 μM), with conductances normalized for each compound to the maximal conductance at +150 mV (*A*) or not normalized (*B*). $n = 6$. Fit functions are presented as Boltzmann fit. (*C* and *D*) Steady-state G–V relationships obtained in HEK293 cells transiently transfected with the TRPM3 pore mutant E1057C in the presence of CIM0216 (1 μM) or PS (40 μM), with conductances normalized for each compound to the maximal conductance at +150 mV (*C*) or not normalized (*D*). $n \geq 8$. (*E* and *F*) Steady-state G–V relationships obtained in HEK293 cells transiently transfected with the S4 mutant W982R in the presence of CIM0216 (1 μM) or PS (40 μM), with conductances normalized for each compound to the maximal conductance at +150 mV (*E*) or not normalized (*F*). $n \geq 5$. The 0-mV conductance was extrapolated from the Boltzmann fit.

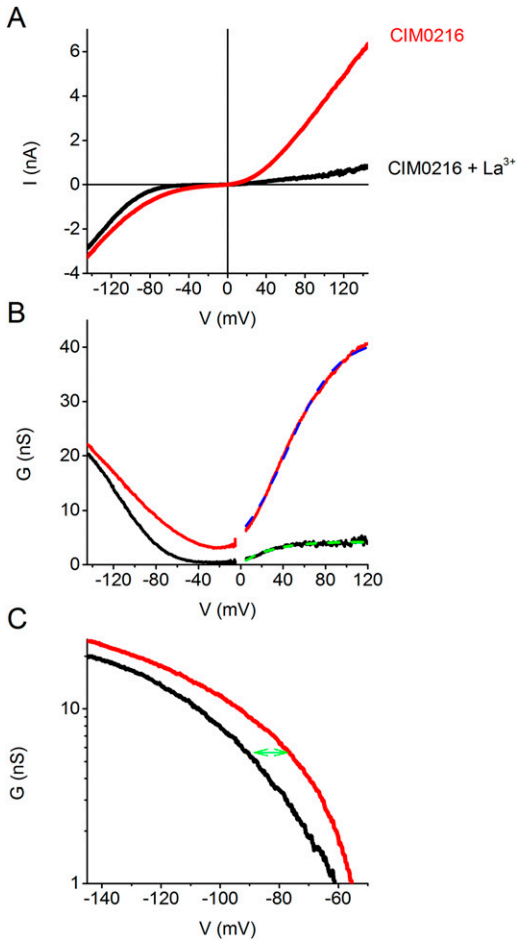

Fig. S7. Effect of La^{3+} on the voltage dependency of the gating-pore current. (*A*) I–V relationships of TRPM3-induced currents after stimulation by CIM0216 in the presence and absence of La^{3+} (100 μM). (*B*) G–V relationships obtained from the current traces shown in *A*. The region between −5 mV and +5 mV was excluded from the analysis. Dashed lines show a Boltzmann function fitted to the rightmost part of the G–V curve (+5 to +120 mV). (*C*) G–V curve of the inwardly rectifying current component. These curves were obtained by subtracting the fitted Boltzmann functions from the total G–V curves shown in *B*.

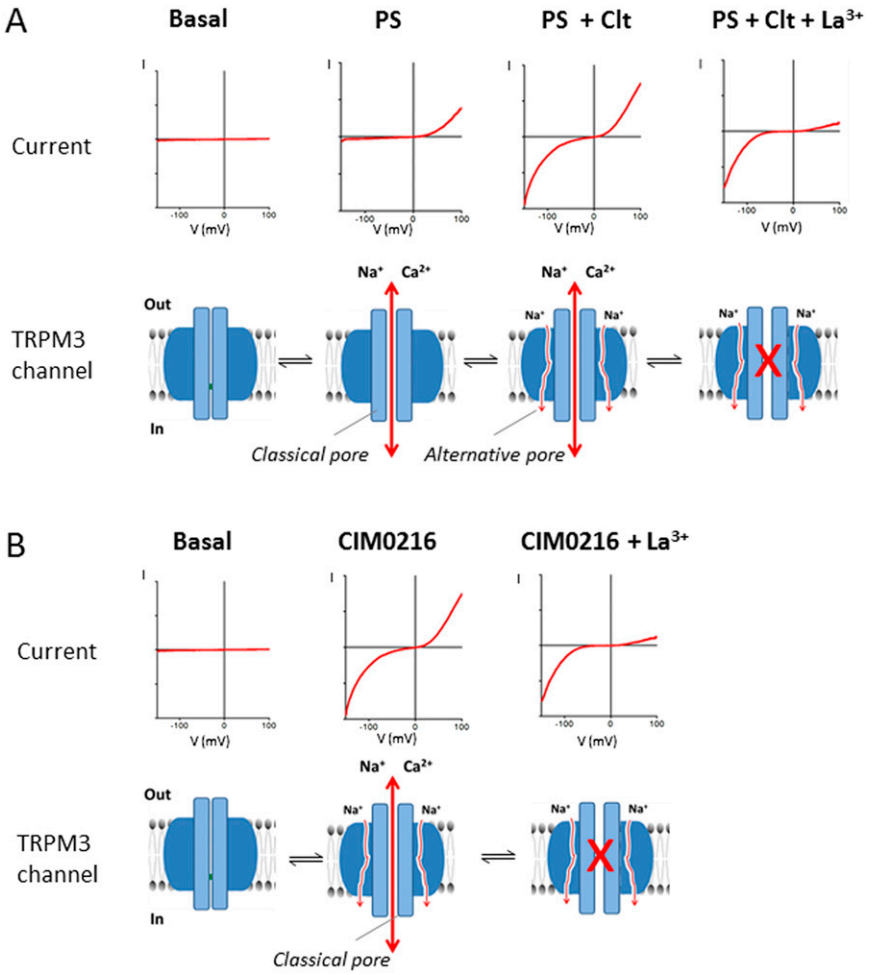

Fig. S8. TRPM3 channels can permeate ions through different pathways. (*A*) PS-activated TRPM3 currents are outwardly rectifying but develop an inwardly rectifying component in response to a combination of the agonist (PS) and the channel modulator Clt. The inwardly rectifying component is not carried by the central pore and is likely to be carried by an alternative ion permeation pathway. Application of the open pore blocker La^{3+} blocks the current through the central pore. (*B*) CIM0216-activated TRPM3 currents are strongly inwardly and outwardly rectifying, even in the absence of the channel modulator Clt. The typically CIM0216-induced rectification pattern is likely to be carried by the opening of the central pore and the alternative pore. La^{3+} blocks the central pore, whereas the alternative ion permeation pathway is unaffected.

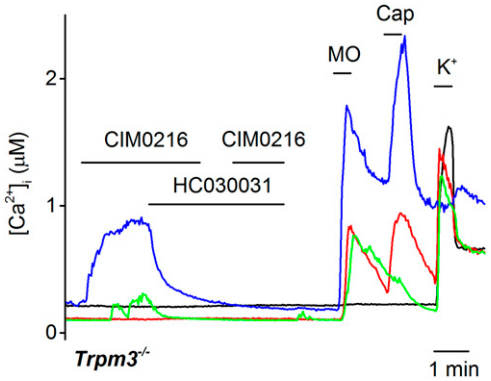

Fig. S9. Selectivity of CIM0216 in sensory neurons. Representative traces showing typical patterns of intracellular Ca^{2+} in DRG and TGN from TRPM3$^{-/-}$ animals in response to CIM0216 (1 μM), the TRPA1 blocker HC030031 (10 μM), MO (100 μM), capsaicin (Cap; 1 μM), and K^+ (50 mM). All sensory TRPM3$^{-/-}$ neurons responding to CIM0216 could be blocked by application of HC030031.

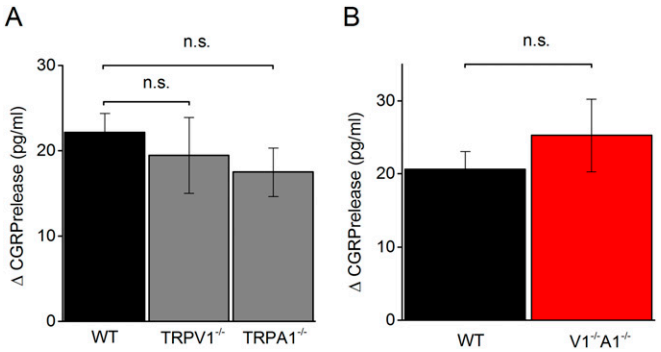

Fig. S10. PS induces CGRP release in the skin preparations of TRPV1$^{-/-}$- and TRPA1$^{-/-}$-deficient mice. (*A*) PS (200 μM) evoked similar increases in the release of CGRP from TRPV1$^{-/-}$ ($n = 5$) and TRPA1$^{-/-}$ ($n = 9$) knockout skin preparations compared with WT skin ($n = 7$). *(B)* CIM0216 (50 μM) induced similar increases in CGRP release in skin preparations from WT and TRPV1$^{-/-}$ TRPA1$^{-/-}$ double-knockout mice ($n = 4$).